Geochemistry Geophysics Geosystems G3
AN ELECTRONIC JOURNAL OF THE EARTH SCIENCES
Published by AGU and the Geochemical Society

Article
Volume 5, Number 12
8 December 2004
Q12005, doi:10.1029/2004GC000789
ISSN: 1525-2027

Short-term variations in the distribution of hydrothermal plumes along a superfast spreading center, East Pacific Rise, 27°30′–32°20′S

Sharon L. Walker and Edward T. Baker
NOAA/Pacific Marine Environmental Laboratory, 7600 Sand Point Way NE, Seattle, Washington 98115, USA (sharon.l.walker@noaa.gov)

Gary J. Massoth
Institute of Geological and Nuclear Sciences, Ltd., 30 Gracefield Road, P.O. Box 31-312, Lower Hutt, New Zealand

Richard N. Hey
Hawaii Institute of Geophysics and Planetology, 2525 Correa Road, University of Hawaii, Honolulu, Hawaii 96822, USA

[1] A multidisciplinary expedition to the southern East Pacific Rise (27°30′–32°20′S) provided an opportunity to compare the efficiency and effectiveness of two methods for mapping hydrothermal plumes: the standard conductivity-temperature-depth-optical (CTDO) tow-yo method and a towed fixed array of hydrographic and optical sensors (Miniature Autonomous Plume Recorders (MAPRs)). Six second-order segments were mapped twice: once with CTDO tow-yos, and then again with a fixed array of MAPRs attached to the cable of a deep-towed side-scan sonar. We found a high degree of overall agreement between the two methods in both the distribution and optical intensity of hydrothermal plumes. Between-survey differences increased as time between surveys increased from <0.5 to >6 days, presumably because of advection of the plumes by local currents. Plume locations changed by as much as ~10 km, implying a confidence limit in predicting vent site location using segment-scale hydrothermal plume surveys. Towed MAPR arrays proved an efficient and effective method for acquiring coregistered geological and hydrothermal plume data.

Components: 4897 words, 4 figures, 1 table.

Keywords: East Pacific Rise; hydrothermal plumes; mapping.

Index Terms: 3035 Marine Geology and Geophysics: Midocean ridge processes; 8135 Tectonophysics: Hydrothermal systems (8424); 8424 Volcanology: Hydrothermal systems (8135).

Received 30 June 2004; **Revised** 2 September 2004; **Accepted** 23 September 2004; **Published** 8 December 2004.

Walker, S. L., E. T. Baker, G. J. Massoth, and R. N. Hey (2004), Short-term variations in the distribution of hydrothermal plumes along a superfast spreading center, East Pacific Rise, 27°30′–32°20′S, *Geochem. Geophys. Geosyst.*, *5*, Q12005, doi:10.1029/2004GC000789.

1. Introduction

[2] Studies examining the distribution of hydrothermal activity along multisegment stretches of the mid-ocean ridge commonly use detailed hydrothermal plume surveys to predict the location of seafloor vent sites and examine the relationship between geological characteristics of mid-ocean ridges and the incidence of hydrothermal activity [*Bougault et al.*, 1990; *Baker et al.*, 1995; *German and Parson*, 1998]. Our knowledge of the global implications of hydrothermal/geological relation-

ships is limited by the small fraction (~10%) of global mid-ocean ridge system that has been surveyed comprehensively to date [*Baker and German*, 2004]. Our ability to estimate the location of vent sites, and thus improve the efficiency of seafloor sampling and imaging studies, is limited because plumes are subject to advection along and across ridge axes in a complex response to near-bottom current flows at tidal and other periods. At any instant a plume may be centered directly over or kilometers away from its source location. High frequency repeat surveys of entire ridge crest segments are rare, but can improve our knowledge of large-scale spatial variability and plume movement over temporal scales of hours to days.

[3] To improve our knowledge of short-term variability in hydrothermal plume distributions, we took advantage of a multidisciplinary study of the superfast spreading East Pacific Rise (EPR) between 27°30′ and 32°20′S that featured repeat surveys of the ridge crest using different tools. The March–April, 1998, RAPA NUI expedition onboard the R/V *Melville* [*Baker et al.*, 2002; *Hey et al.*, 2004] conducted two systematic surveys of six second-order segments, with a time lag of <0.5–>6 days between surveys on each segment. Each segment was surveyed once for hydrothermal plumes using a standard conductivity/temperature/depth/optical (CTDO) tow-yo [*Baker et al.*, 1995] and again for high-resolution acoustical imagery using the WHOI DSL-120 kHz deep-towed side-scan sonar system with up to six Miniature Autonomous Plume Recorders (MAPRs) [*Baker and Milburn*, 1997] attached. Both the CTDO and DSL-120/MAPR surveys were enhanced by the addition of the PMEL SUAVE, an in situ chemical analyzer that measures Fe, Mn, and hydrographic parameters, including light backscattering, which provided additional chemical characterization of plumes as they were mapped [*Massoth et al.*, 1998; *Massoth and Hey*, 1998; *Hey et al.*, 2004].

[4] The MAPR is a hydrographic and optical recorder designed to detect plumes in conjunction with operations such as rock (wax) cores, dredges, and deep-towed geophysical and bottom imaging packages where a wire is lowered to the seafloor but no water column data are usually recovered. MAPRs have been used on each of these kinds of operations to detect hydrothermal plumes in a wide variety of geological settings [*Scheirer et al.*, 1998; *German et al.*, 1998, 2000; *Baker et al.*, 2001a], and are proving to be efficient tools for maximizing plume survey opportunities. In this paper we make a detailed comparison of the results of plume surveys from CTDO and MAPR tows to verify that utilizing multiple MAPR sensors on a deep tow cable is comparable to CTDO surveys for detecting and mapping hydrothermal plumes. We evaluate the variability in plume distributions revealed by the repeat surveys and define confidence limits for estimating vent locations on the seafloor from segment-scale plume surveys.

2. Methods

2.1. Study Area

[5] The large non-transform offset between the Easter and Juan Fernandez microplates on the southern EPR consists of two limbs of a dual propagating rift system [*Naar and Hey*, 1991; *Hey et al.*, 1995; *Korenaga and Hey*, 1996]. Spreading rates range from 0 to ~150 mm/yr, the fastest anywhere in the world. The east and west ridges form a large overlapping spreading system between about 28°30′S and 29°30′S with a separation of 120 km (Figure 1). The west and east ridges are each divided into four segments by second-order overlapping spreading centers (OSC), designated W1 through W4 and E1 through E4, respectively, that are separated by 1–7 km widths over distances of 2–14 km [*Martínez et al.*, 1997; *Korenaga and Hey*, 1996]. *Hey et al.* [2004] describe discontinuities that further divide these segments into subsegments delineated by non-intersecting rift zones or inflation boundaries. Segments W3, W4, and E1 through E4 were surveyed in their entirety during this expedition. The cross-sectional area [*Scheirer and Macdonald*, 1993] for individual segments varies from ~0 to >8 km^2, and axial depths vary from 2100 to 2960 m [*Martínez et al.*, 1997] (Figure 2). *Baker et al.* [2002] and *Hey et al.* [2004] discuss the relationship of hydrothermal venting to the variable geology along these segments.

2.2. CTDO Tow-Yos

[6] CTDO tow-yos used a high-precision Sea Bird 911*plus* CTD with a light-backscattering sensor (LBSS). LBSS measurements are relative rather than absolute measures of the light backscattering coefficient and can differ slightly among individual sensors [*Baker et al.*, 2001b]. We report our results in terms of nephelometric turbidity units (NTUs) according to the expression

$$\Delta\mathrm{NTU} = (V_r - V_b)/a_n,$$

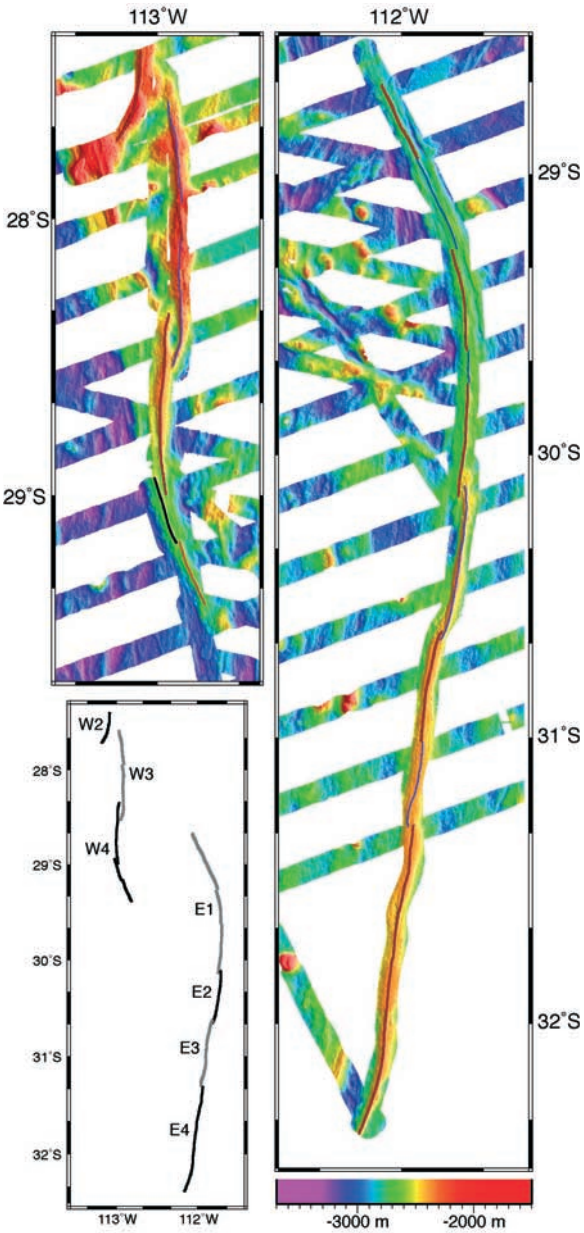

Figure 1. Ridgecrest bathymetry of the six segments surveyed. SeaBeam data from *Hey et al.* [1995] and *Martínez et al.* [1997], augmented by new data from RAPA NUI expedition [*Baker et al.*, 2002].

where ΔNTU is the plume LBSS anomaly relative to ambient seawater, V_r is the raw voltage reading of the LBSS, V_b is the background voltage of ambient water not affected by hydrothermal plumes, and a_n is a factor unique to each LBSS determined from a laboratory calibration using formazine [*Baker et al.*, 2001b]. LBSS response is from 0–5v, and field calibrations have shown that for typical deep-sea particles, the mass concentration, C_m, is related to ΔNTU by $C_m = -0.003 + 0.39(\Delta NTU)$, $r^2 = 0.97$ [*Baker et al.*, 2001b]. Confidence limits on the slope at the 95% level are ±0.019. The confidence interval (at the 95% level) for predicting C_m is ±0.004 mg/l for a ΔNTU of 0.1 and ±0.008 mg/l for a ΔNTU of 0.3.

[7] The CTDO tow-yo traces a sawtooth path along the trackline by vertically cycling the instrument/bottle package through the bottommost ~500 m as the ship steams ahead at 2–3 km/hr. For this study, 24 Hz CTDO data were averaged over 5 s intervals yielding data resulting in a vertical spacing of 5–10 m with maximum depths to within 10–20 m of the seafloor and minimum depths determined by real-time observation of ambient seawater above all plume anomalies. The wavelength of the vertical legs of the sawtooth path was 0.5–1 km.

2.3. Fixed MAPR Array/Side-Scan Sonar Tow

[8] MAPRs are lightweight, rugged, and uncomplicated self-contained instruments for recording temperature, pressure and optical data in conjunction with a wide variety of oceanographic operations [*Baker and Milburn*, 1997]. Temperature is recorded using a YSI 46006 thermistor (0.001°C resolution, 2.5 s maximum time constant) mounted in a titanium probe extending from the top end cap. A Paine strain gauge sensor with a range of 0–33,775 kPa (minimum) and a resolution of 1.35 kPa (0.135 db) measures pressure. A LBSS, the same type as on the CTDO package, senses backscattered light. ΔNTU is calculated in the same manner as for the CTDO tow-yos.

[9] As many as six MAPRs were attached to the tow cable of the DSL-120 side-scan sonar, including one unit suspended 40 m below the depressor weight (Figure 3). An additional LBSS sensor was mounted on the weight itself as part of the PMEL SUAVE in-situ chemical analyzer [*Massoth et al.*, 1998; *Massoth and Hey*, 1998]. The DSL-120 was towed at a nominal height of 100 m above bottom at 2–3 km/hr. Data were thus acquired along fixed parallel paths above and below the DSL-120 within the depth range of 60 to 300 m above bottom (and to 420 mab on W3). A 15 s sampling interval provided horizontally spaced records approximately every 10 m at the normal DSL-120 tow speed.

3. Results

[10] Over 600 km of axis were completely surveyed twice during the cruise. For both the MAPR

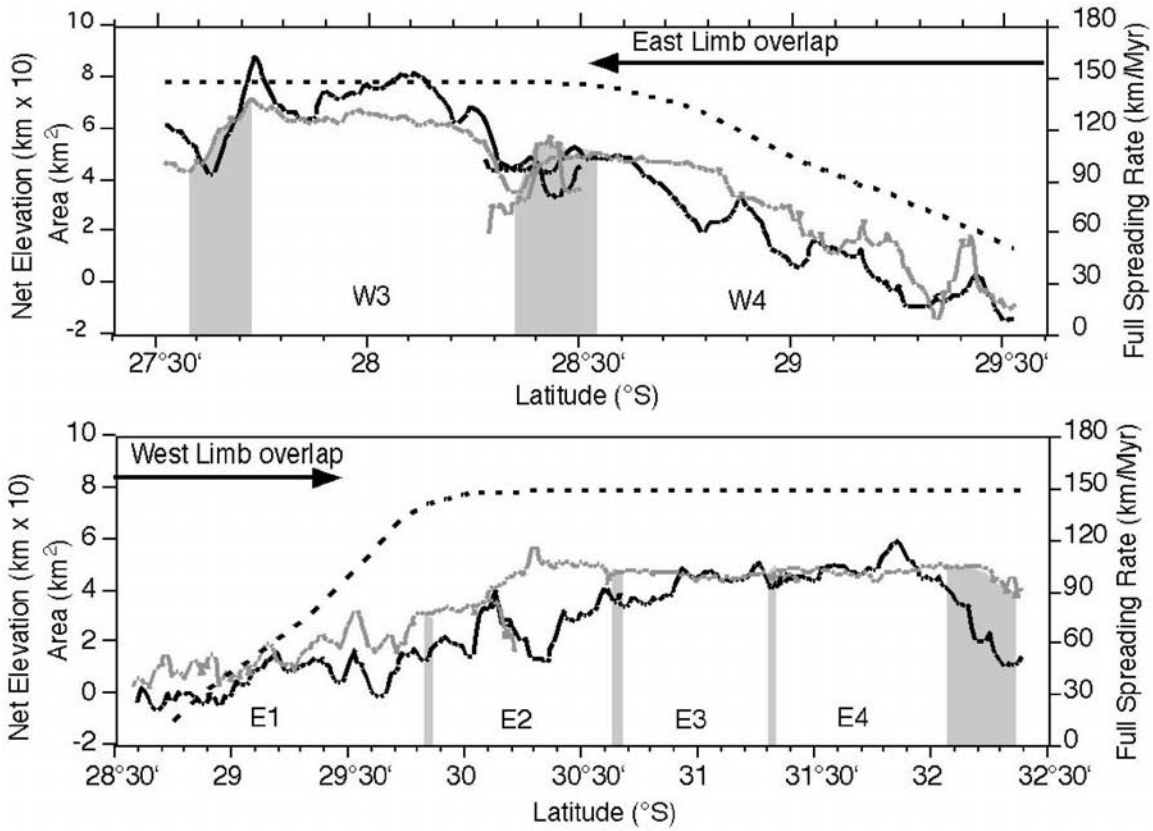

Figure 2. Along-axis trends in full spreading rate (dashed line), net elevation of the ridge axis (gray solid line), and the cross-sectional area of the ridge crest (dark solid line) for the west (top) and east (bottom) ridges. Extent of OSCs separating each segment indicated by shaded zones, and extent of the overlapping dueling propagators marked by arrows at the top of each panel [after *Baker et al.*, 2002].

and CTDO surveys, plumes are imaged as ΔNTU values plotted as individual data points scaled by color (Figure 3). This technique, compared to contouring the data, better visualizes detailed differences between the two types of surveys at multisegment scales. Both surveys detected hydrothermal plumes on each segment and displayed similar intensities and overall distributions. The most concentrated and continuous plumes were found along segments W3/W4 from 27°40′S to 28°44′S, and segments E3/E4 from 31°00′S to 31°58′S. Segments E1 and E2 had generally weaker hydrothermal signals, and neither survey detected substantial plumes along the overlapping propagators of both ridges where spreading rates and ridge cross-sectional inflation are low (Figure 2).

[11] Beyond this overall agreement, we found noticeable differences in the details of the plume distribution mapped from each survey. These differences include minor changes in the vertical and horizontal plume structure, lateral displacement of plumes by several kilometers, and plumes observed on only one of the surveys. Fine-scale differences in the plume structure and intensity are inevitable given that the MAPR data are high-resolution in the horizontal whereas the CTDO data are high-resolution in the vertical. To illustrate these differences we plotted the section of segment E3 between 31°00′ and 31°18′S on an expanded scale as a contour plot (Figure 4). An active hydrothermal source near 31°09′S was first identified from a near-bottom density inversion (interpreted as a buoyant plume) detected during the CTDO tow, and confirmed in January 1999 by the discovery of a high-temperature vent field at 31°09′S [*Lupton et al.*, 1999]. The time difference between CTDO and MAPR surveys along this portion of segment E3 ranged from 0.3 to 1.2 days, the tows were conducted in opposite directions with the CTDO survey occurring first. Both transects yield downward inflection of the ΔNTU

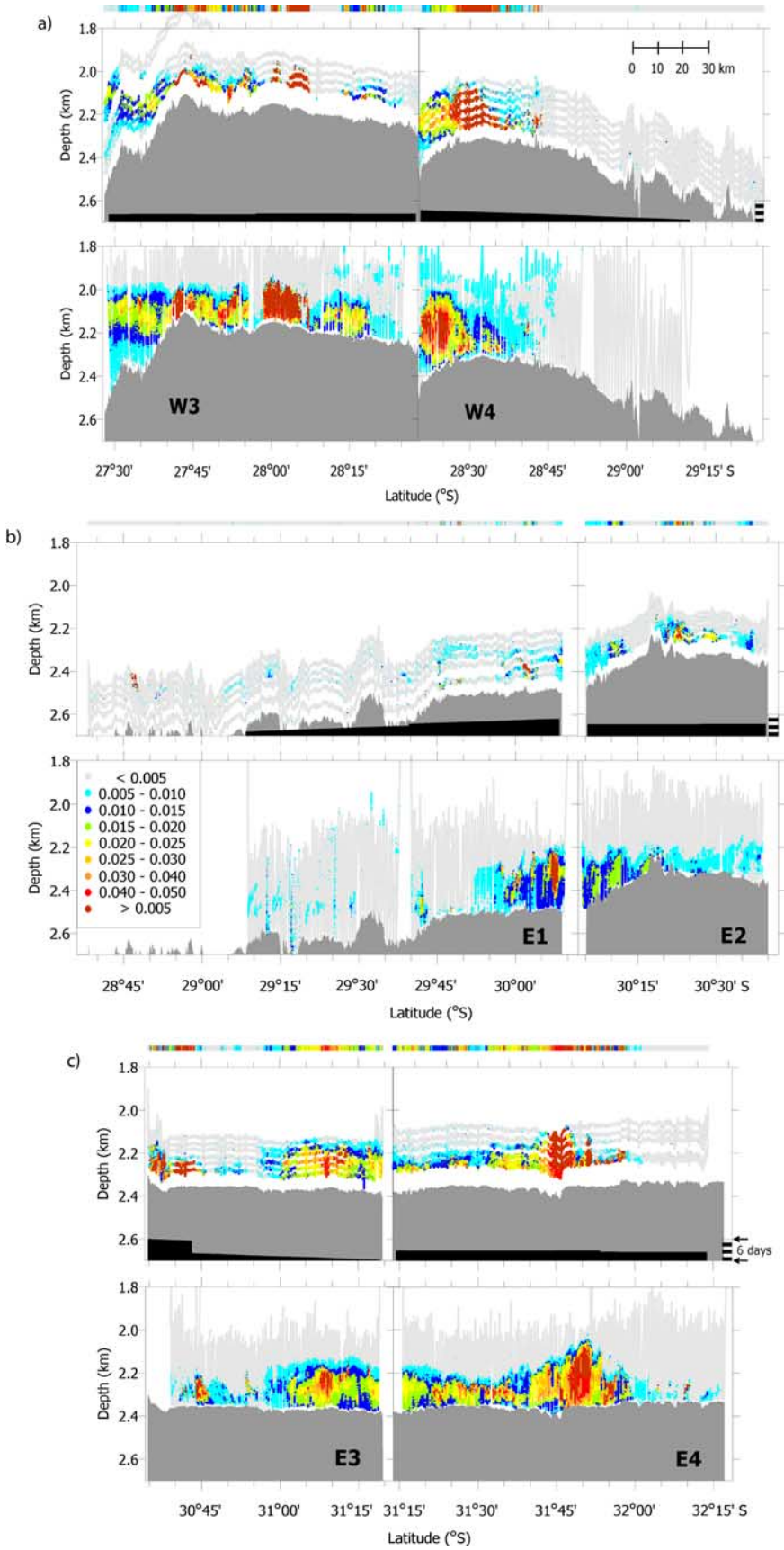
a)
0 10 20 30 km
Depth (km)
W3
W4
27°30' 27°45' 28°00' 28°15' 28°30' 28°45' 29°00' 29°15' S
Latitude (°S)
b)
< 0.005
0.005 - 0.010
0.010 - 0.015
0.015 - 0.020
0.020 - 0.025
0.025 - 0.030
0.030 - 0.040
0.040 - 0.050
> 0.005
E1
E2
28°45' 29°00' 29°15' 29°30' 29°45' 30°00' 30°15' 30°30' S
Latitude (°S)
c)
6 days
E3
E4
30°45' 31°00' 31°15' 31°15' 31°30' 31°45' 32°00' 32°15' S
Latitude (°S)

Figure 3

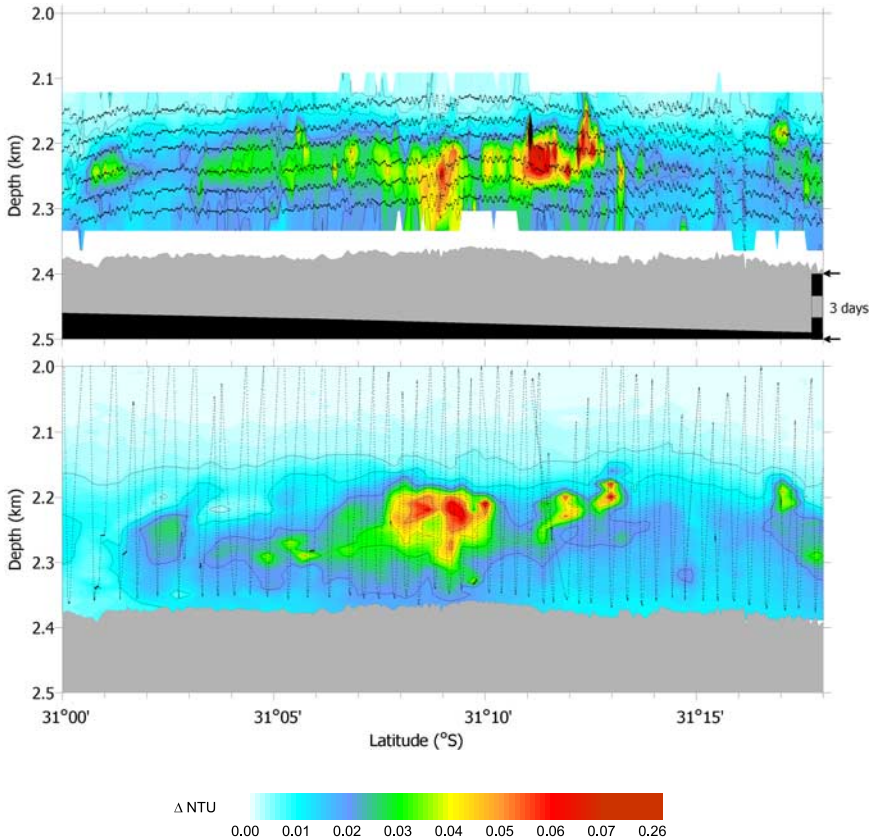

Figure 4. Contour plot of (top) MAPR and (bottom) CTDO ΔNTU data from a portion of segment E3. Black dots show actual location of data points within the gridded field. Grid line spacing for MAPR plot is x = 100 m, y = 30 m. Grid line spacing for CTDO plot is x = 500 m, y = 10 m. Time difference between the initial CTDO tow and the subsequent MAPR tow is shown as black block at the bottom of the MAPR frame. A high-temperature vent field was discovered at 31°09′ in 1999 [*Lupton et al.*, 1999].

contours, indicating a dispersing plume fed by the seafloor hydrothermal source near 31°09′S, but in the MAPR survey the plume appears somewhat thicker and more continuous between 31°03′S to 31°06′S and 31°09′S to 31°10.5′S. These differences are likely a function of both contrasting resolution between the two methods and the elapsed time between surveys. Plume similarities are greatest where the time difference is smallest (0.3 days at 31°18′S) and least where the time difference is largest (1.2 days at 31°00′S), but the overall extent and intensity of the plume are quite similar. Integration of ΔNTU values for each found a difference of <20% between the two sections.

[12] The vertical range of MAPR surveys is limited by the number of available instruments, their placement along the tow cable, and the optimal operating distance above bottom required for the DSL-120. In contrast, the real-time monitoring and vertical mobility of CTDO surveys enable operators to fully cycle the sensors between very near the seafloor and well above any observed tracer anomalies to completely define the vertical extent of the plumes.

Figure 3. MAPR (top panels) and CTDO (bottom panels) ΔNTU data along (a) west ridge segments W3 and W4, (b) east ridge segments E1 and E2, and (c) east ridge segments E3 and E4. Black blocks at the base of each MAPR panel show the time difference between MAPR and CTDO tows (0–6 day range). The color bar at the top of each segment shows data from the SUAVE LBSS mounted on the DSL-120 depressor weight and towed 100 m above bottom. MAPRs were vertically spaced on the tow wire above the depressor weight at 20–40 m intervals. No MAPR was hung below the depressor weight for the tows along segments W3 and E4. The truncated record and data gaps along segment W3 were due to LBSS bracket damage on three of the MAPRs. The high ΔNTU values at the very north end of segment E1 during the MAPR survey are due to separate, brief periods of noise in two different LBSS records. ΔNTU scale is shown in Figure 3b.

For example, for operational reasons we hung no MAPR below the clump weight of the DSL-120 along segments W3 and E4, so plume information is lacking for the lowermost 100 m, markedly compromising the imaging of the near-bottom plumes (Figure 3). On segments E3 and E4 we likely missed the top of some of the highest-rising plumes. While these differences in data distribution provide different views of plume structure, they cannot account for the displacement or presence/absence of entire plumes between surveys.

[13] Large-scale differences appear to be related to the time difference between the two surveys at any given ridge location, which ranged from <0.5 days to >6 days (Figure 3). Segments where both tows were conducted in the same direction have a uniform time difference (W3, E2, E4), whereas those with tows in opposing directions have strongly varying differences that increase with the length of a segment (W4, E1, E3).

[14] The best agreement in the location and extent of intense plumes between MAPR and CTDO surveys occurred along segments W3 and most of E3 where the time between surveys was 2 days or less. Robust plumes centered at 27°44′S (W3), 27°52′S (W3), 28°03′S (W3), and 31°09′S (E3) changed little in intensity or location between surveys. By comparison, CTDO-located plumes centered at 28°24′S (W4) and 31°50′S (E4) were noticeably displaced in the MAPR surveys about 3 days later. The W4 plume migrated 11 km south from 28°24′S to 28°30′S over 3.4 days, while the E4 plume migrated 9 km north from 31°50′S to 31°45′S over 2.7 days. Net speed for both migrations was ~3.8 cm/s, a reasonable value for near-bottom ridge crest currents over time spans longer than tidal and inertial periods [*Crane et al.*, 1988; *Thomson et al.*, 1990; *Cannon and Pashinski*, 1997]. Note, however, that this estimate includes only the along-axis component of flow.

[15] Distinct differences can also be seen on segments E1 and E2 where the time interval between surveys exceeds ~3 days. On segment E1, the MAPR survey found only a small but intense signal at ~30°02′S and perhaps the edge of a plume at the end of the tow at 30°09′S. A CTDO survey 4–5 days later also detected a single plume but somewhat farther south at 30°07.5′S, though this plume may in fact be the same feature barely imaged at 30°09′S during the MAPR tow. Plumes over segment E2 were similar during both surveys except for some minor plume maxima near 30°23′S seen only on the MAPR tow.

[16] One of the most significant differences between the MAPR and CTDO surveys occurred along the E2/E3 OSC. Comparisons here are difficult, however, as the CTDO and MAPR tow paths did not precisely overlap. Because of the small size of this OSC, a maximum 1.5 km separation across an axial length of 3.5 km, the CTDO towpath followed neither limb but passed from E2 to E3 over the OSC basin. The DSL-120/MAPR array was towed separately over the axial delineations for both E2 and E3. The absence of a strong plume over the eastern limb and basin of the OSC (i.e., CTDO and MAPR tows on E2) but an intense plume on the western side (i.e., MAPR tow on E3) suggests that E3 but not E2 hosts hydrothermal activity here, and that no easterly component to the deep local flow was active during our observations. A similar plume asymmetry has been documented on cross-axis tows at other locations on the northern [*Baker et al.*, 1994] and southern [*Baker and Urabe*, 1996] EPR. The lag of 6 days between the CTDO and MAPR surveys at the northern end of E3 was the greatest of the cruise and could also be a factor in the dissimilarity of plume distributions along this section. The CTDO tow-yo for the remainder of E3 (south of ~30°44′S) began less than 2 days prior to the MAPR survey, and also shows evidence of the strong plume in the area of the OSC observed by the MAPRs.

[17] Despite the short-term variations in plume distributions between the MAPR and CTDO surveys, we observed little difference in the total extent of plume coverage over the entire survey area. For each survey, we calculated plume incidence (p_h) [*Baker and Hammond*, 1992; *Baker et al.*, 1994, 1996, 2004] as the fraction of linear ridge axis overlain by significant plumes, an inferential index of the extent of hydrothermal vent fields on the seafloor. Identification of "significant" plumes is unavoidably subjective, and in this study we use ΔNTU values greater than a threshold value of 0.015 for calculating p_h. Optical anomaly gradients at the edges of most plumes are sharp, so determination of p_h is not highly sensitive to the threshold value. The value selected here effectively filters out low-level background noise in the LBSS signal and ignores the most dilute edges of the dispersing plumes which are not likely to be located directly over seafloor discharge sites. Plume incidence for the entire study area during the MAPR survey was 0.47 while the CTDO survey yielded a p_h of 0.43 (Table 1). When only the portions of the east and west ridges with full

Table 1. Plume Incidence (p_h) Calculated for CTDO, Multiple MAPR, and Single MAPR Surveys

Segment	Segment Length, km	CTDO p_h	Multiple MAPR p_h	Single MAPR p_h
W3	112	0.72	0.73	0.60
W4 (whole)	122	0.25	0.38	0.34
W4 (<130 km/Ma)	71	0.00	0.03	0.00
W4 (>130 km/Ma)	51	0.60	0.85	0.81
E1 (whole)	168	0.12	0.10	0.09
E1 (<130 km/Ma)	118	0.00	0.03	0.00
E1 (>130 km/Ma)	50	0.39	0.28	0.28
E2	64	0.36	0.42	0.26
E3	83	0.55	0.72	0.63
E4	111	0.77	0.68	0.68
Total	660	0.43	0.47	0.41
<130 km/Ma	189	0.00	0.03	0.00
>130 km/Ma	471	0.60	0.64	0.57

spreading rates >130 km/Ma are considered, p_h increases to 0.64 and 0.60 for the MAPR and CTDO surveys, respectively. These results closely agree with the value of 0.60 found for plumes overlying the superfast spreading EPR between 13°50′S and 18°40′S [*Baker and Urabe*, 1996], and support the hypothesis of a linear relation between p_h and spreading rate, a proxy for the long-term magmatic budget of a multisegment ridge section [*Baker and Hammond*, 1992; *Baker et al.*, 1996; *Baker and German*, 2004]. Moreover, the good agreement between the two surveys greatly improves our confidence that a single detailed survey can provide a reliable view of large-scale plume distributions.

[18] Since a full suite of MAPRs may not be available for every study, we calculated p_h using ΔNTU from only a single horizon to see what effect having just one MAPR would have on the ability to determine a representative p_h value. We chose the LBSS integrated with SUAVE and mounted on the DSL-120 depressor weight towed at 100 m above bottom because the experience of this survey, as well as many others [*Baker et al.*, 1995], shows this level is most likely to fall within the plume core. The p_h at this distance above bottom was 0.41 for the total length of ridge sampled and 0.57 for that portion with >130 km/Ma spreading rate, comparable to the values calculated when using all available sensors.

4. Conclusions

[19] MAPRs offer a means to detect hydrothermal plumes during oceanographic operations where water column data are not normally collected. An array of MAPRs fixed at several depths on a deep-tow cable can describe the overall distribution and intensity of hydrothermal plumes on segment-scale surveys in detail comparable to CTDO tow-yos. Plume distributions during this expedition were fundamentally similar, except some plume locations changed by as much as ∼10 km, presumably the result of advection by local currents. On the basis of this variability, confidence in assigning positions to undiscovered vent fields using only the locations of neutrally buoyant plumes observed on a single CTDO or MAPR survey would be no better than ∼10 km. CTDO tows are more suitably equipped to detect near-bottom density inversions caused by buoyant plumes, which can pinpoint active discharge locations. With the MAPR/side-scan sonar combination, however, plume distribution is simultaneously acquired with seafloor geological imagery, making for a very efficient sampling strategy.

[20] The ability to determine segment-scale values of plume incidence is comparable between CTDO tow-yos and fixed MAPR array tows, and even a single MAPR towed at the typical plume height for this region (∼100 m above bottom) can provide a useful estimate of the plume distribution comparable to more detailed surveys.

Acknowledgments

[21] This work was funded by the NOAA VENTS program and by NSF Program grants OCE-9529737 and OCE-9906896. Special thanks go to Hugh Milburn, Chris Meinig, Pat McLain, and Dennis Holzer for designing and building the MAPRs. The officers and crew of the R/V *Melville* and the engineers and technicians of the WHOI DSL-120 group made

these studies possible. Contribution 2396 from NOAA Pacific Marine Environmental Laboratory and 6428 from SOEST.

References

Baker, E. T., and C. R. German (2004), On the global distribution of hydrothermal vent fields, in *Mid-Ocean Ridges: Hydrothermal Interactions Between the Lithosphere and Oceans*, *Geophys. Monogr. Ser.*, vol. 148, edited by C. R. German, J. Lin, and L. M. Parson, pp. 245–266, AGU, Washington, D. C.

Baker, E. T., and S. R. Hammond (1992), Hydrothermal venting and the apparent magmatic budget of the Juan de Fuca Ridge, *J. Geophys. Res.*, *97*, 3443–3456.

Baker, E. T., and H. B. Milburn (1997), MAPR: A new instrument for hydrothermal plume mapping, *RIDGE Events*, *8*, 23–25.

Baker, E. T., and T. Urabe (1996), Extensive distribution of hydrothermal plumes along the superfast-spreading East Pacific Rise, 13°50′–18°40′S, *J. Geophys. Res.*, *101*, 8685–8695.

Baker, E. T., R. A. Feely, M. J. Mottl, F. J. Sansone, C. G. Wheat, J. A. Resing, and J. E. Lupton (1994), Hydrothermal plumes along the east Pacific Rise, 8°40′ to 11°50′N: Plume distribution and relationship to the apparent magmatic budget, *Earth Planet. Sci. Lett.*, *128*, 1–17.

Baker, E. T., C. R. German, and H. Elderfield (1995), Hydrothermal plumes over spreading-center axes: Global distributions and geological inferences, in *Seafloor Hydrothermal Systems: Physical, Chemical, Biological, and Geological Interactions*, *Geophys. Monogr. Ser.*, vol. 91, edited by S. Humphris et al., pp. 47–71, AGU, Washington, D. C.

Baker, E. T., Y. J. Chen, and J. Phipps Morgan (1996), The relationship between near-axis hydrothermal cooling and the spreading rate of mid-ocean ridges, *Earth Planet. Sci. Lett.*, *142*, 137–145.

Baker, E. T., M. Cormier, C. H. Langmuir, and K. Zavala (2001a), Hydrothermal plumes along segments of contrasting magmatic influence, 15°20′–18°30′N, East Pacific Rise: Influence of axial faulting, *Geochem. Geophys. Geosyst.*, *2*, doi:10.1029/2000GC000165.

Baker, E. T., D. A. Tennant, R. A. Feely, G. T. Lebon, and S. L. Walker (2001b), Field and laboratory studies on the effect of particle size and composition on optical backscattering measurements in hydrothermal plumes, *Deep Sea Res., Part I*, *48*, 593–604.

Baker, E. T., et al. (2002), Hydrothermal venting along Earth's fastest spreading center: East Pacific Rise, 27.5°–32.3°S, *J. Geophys. Res.*, *107*(B7), 2130, doi:10.1029/2001JB000651.

Baker, E. T., H. N. Edmonds, P. J. Michael, W. Bach, H. J. B. Dick, J. E. Snow, S. L. Walker, N. R. Banerjee, and C. H. Langmuir (2004), Hydrothermal venting in magma deserts: The ultraslow-spreading Gakkel and Southwest Indian Ridges, *Geochem. Geophys. Geosyst.*, *5*, Q08002, doi:10.1029/2004GC000712.

Bougault, H., J. L. Charlou, Y. Fouquet, and H. D. Needham (1990), Activité hydrothermale et structure axiale des dorsales Est-Pacifique et médio-Atlantique, *Oceanol. Acta*, *10*, special issue, 199–207.

Cannon, G. A., and D. J. Pashinski (1997), Variations in mean currents affecting hydrothermal plumes on the Juan de Fuca Ridge, *J. Geophys. Res.*, *102*, 24,965–24,976.

Crane, K., F. A. Aikman III, and J.-P. Foucher (1988), The distribution of geothermal fields along the East Pacific Rise from 13°10′N to 8°20′N: Implications for deep-seated origins, *Mar. Geophys. Res.*, *9*, 211–236.

German, C. R., and L. M. Parson (1998), Distributions of hydrothermal activity along the Mid-Atlantic Ridge: Interplay of magmatic and tectonic controls, *Earth Planet. Sci. Lett.*, *160*, 327–341.

German, C. R., E. T. Baker, C. Mevel, K. Tamaki, and FUJI Scientific Team (1998), Hydrothermal activity along the southwest Indian Ridge, *Nature*, *395*, 490–493.

German, C. R., R. A. Livermore, E. T. Baker, N. I. Bruguier, D. P. Connelly, A. P. Cunningham, P. Morris, I. P. Rouse, P. J. Statham, and P. A. Tyler (2000), Hydrothermal plumes above the East Scotia Ridge: An isolated high-latitude back-arc spreading centre, *Earth Planet. Sci. Lett.*, *184*, 241–250.

Hey, R. N., P. D. Johnson, F. Martinez, J. Korenaga, M. L. Somers, Q. J. Huggett, T. P. LeBas, R. I. Rusby, and D. F. Naar (1995), Plate boundary reorganization at a large-offset, rapidly propagating rift, *Nature*, *378*, 167–170.

Hey, R. N., et al. (2004), Tectonic/volcanic segmentation and controls on hydrothermal venting along Earth's fastest seafloor spreading system, EPR 27°–32°S, *Geochem. Geophys. Geosyst*, in press, doi:10.1029/2004GC000764.

Korenaga, J., and R. N. Hey (1996), Recent dueling propagation history at the fastest spreading center, the East Pacific Rise, 26°–32°S, *J. Geophys. Res.*, *101*, 18,023–18,041.

Lupton, J., D. Butterfield, M. Lilley, J. Ishibashi, D. Hey, and L. Evans (1999), Gas chemistry of hydrothermal fluids along the East Pacific Rise, 5°S to 32°S, *Eos Trans. AGU*, *80*(46), Fall Meet. Suppl., F1099.

Martínez, F., R. N. Hey, and P. D. Johnson (1997), The East ridge system 28.5°–32°S East Pacific Rise: Implications for overlapping spreading center development, *Earth Planet. Sci. Lett.*, *151*, 13–31.

Massoth, G. J., and R. N. Hey (1998), SUAVE perspectives on the southern East Pacific Rise, *Eos Trans. AGU*, *79*(45), Fall Meet. Suppl., F831.

Massoth, G. J., E. T. Baker, R. A. Feely, J. E. Lupton, R. W. Collier, J. F. Gendron, K. K. Roe, S. M. Maenner, and J. A. Resing (1998), Manganese and iron in hydrothermal plumes resulting from the 1996 Gorda Ridge event, *Deep Sea Res., Part II*, *45*, 2683–2712.

Naar, D. F., and R. N. Hey (1991), Tectonic evolution of the Easter microplate, *J. Geophys. Res.*, *96*, 7961–7993.

Scheirer, D. S., and K. C. Macdonald (1993), The variation in cross-sectional area of the axial ridge along the East Pacific Rise: Evidence for the magmatic budget of a fast-spreading center, *J. Geophys. Res.*, *98*, 7871–7885.

Scheirer, D. S., E. T. Baker, and K. T. M. Johnson (1998), Detection of hydrothermal plumes along the southeast Indian Ridge near the Amsterdam–St. Paul Plateau, *Geophys. Res. Lett.*, *25*, 97–100.

Thomson, R. E., S. E. Roth, and J. Dymond (1990), Near-inertial motions over a mid-ocean ridge: Effects of topography and hydrothermal plumes, *J. Geophys. Res.*, *95*, 7261–7268.